Applications of One-Dimensional Bubbles to Lithotripsy, and to Diver Response to Low Frequency Sound

T.G. Leighton, P.R. White and M.A. Marsden

Institute Sound and Vibration Research, University of Southampton, SO17 1BH, UK

(Received 8 June 1995; accepted 27 September 1995)

Abstract. — Experimental, analytical, and numerical investigations into the dynamics of a cylindrical gas pocket in a liquid (a "one-dimensional" bubble) are described. One wall of the bubble (the gas-liquid interface) may move. The other walls (the curved wall, and the other end of the cylinder) are bounded by rigid surfaces. The equation of motion of a damped, forced, one-dimensional bubble is obtained, a nonlinearity arising through the amplitude-dependence of the oscillator stiffness. Analytical solutions to reduced forms of this equation give the natural frequency of undamped oscillations in the linear limit. In the nonlinear regime of finite-amplitude free oscillation the fundamental frequency is found to be amplitude-dependent. Whilst analytical solutions of the undamped, unforced form of the equation of motion can be obtained in phase space, the full nonlinear damped forced equation must be solved numerically. These solutions are compared with those of the linear undamped analysis, and with experimental measurements. Two relevant cases of such bubbles are studied: First, air bubbles trapped within the ear canals of divers and driven by high-amplitude low frequency sound; second, the theoretical potential of bubbles in blood to cause haemorrhage of lung blood vessels during lithotripsy.

Pacs numbers: 43.30Lz — 43.25Yw.

1. Introduction

Analysis of the dynamics of cylindrical pockets of gas within rigid tubes reveals several features of use for indicating the possible consequences of subjecting bubbles in the ear canals of divers, or within blood capillaries, to intense sound fields. In the simplest model the velocity associated with the meniscus is in one Cartesian dimension only, so that this bubble is loosely termed "one-dimensional". This is to distinguish it from three-dimensional bubbles[1], the significant difference being in the way geometrical spreading allows fluid motion to diverge away from the bubble in the three-dimensional case, but not in the one-dimensional. This means that the inertia associated with the volume changes in a truly one-dimensional bubble is undefined, which has consequences for the dynamics of bubbles subjected to pressure changes in pipes which are of comparable diameter with that of the bubble, but which are very long. The case of blood vessels is examined. However, many practical examples of these bubbles are not truly one-dimensional, in that the geometry does diverge some distance away from the bubble. In such circumstances the inertia associated with oscillation (the "radiation mass") is finite, and the bubble acts as an oscillator.

Such divergence is incorporated within the model one-dimensional bubble discussed here, the liquid some distance from the gas space diverging from a tube into a cone geometry (Figure 1), where the liquid velocity field resembles that found in a spherically-diverging geometry. In this way, the inertia is finite, and the natural frequencies of the bubble are found in the limit of harmonic, small-amplitude oscillations. The analysis also allows consideration of the stiffness term, and the equation of motion is constructed. Whilst analytical solutions in phase space may be obtained for undamped free oscillations, numerical techniques are required for the full equation. The predictions are compared with experimental measurement of a one-dimensional bubble. Resonances associated with membrane oscillations are also discussed, and likely resonances of air bubbles in the ear canals of divers are studied.

[1]Spherical bubbles are the symmetrical limiting case of three-dimensional bubbles, illustrating the figurative, rather than the definitive, nature of the terminology. Ideally fluid motion about a pulsating sphere is in one spherical dimension only, the radial, but in three Cartesian dimensions.

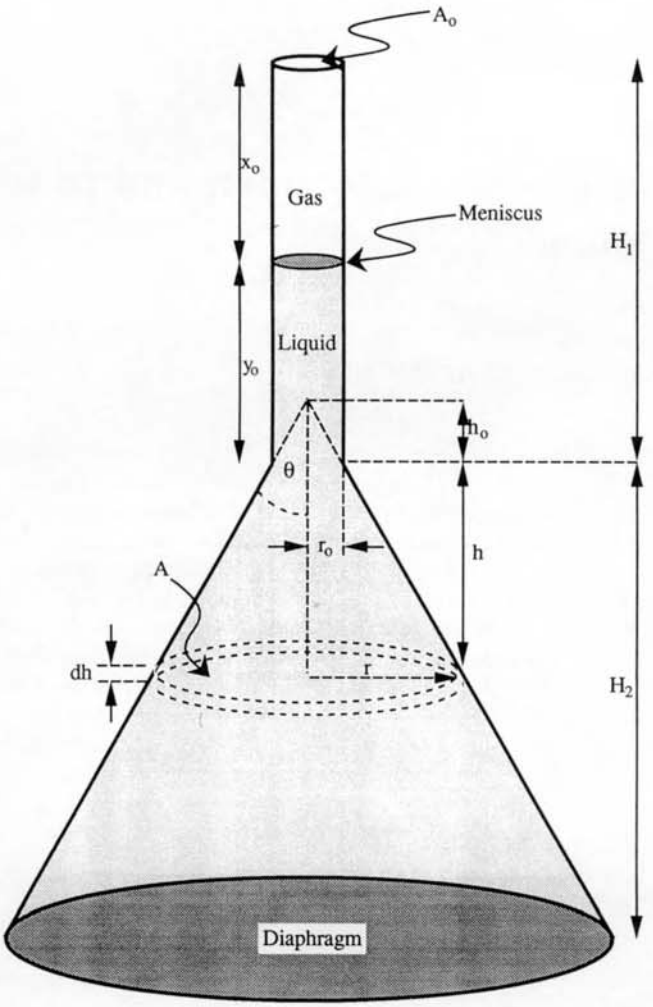

Figure 1. Schematic of 1-D bubble.

2. Theory

The natural frequency of the undamped one-dimensional bubble can be calculated by equating the maximum potential energy (associated primarily with the gas) with the maximum kinetic energy (invested primarily in the liquid). Initially, surface tension, friction and viscous effects are ignored, as is the possibility of meniscus deformation. To find the potential energy of the gas, assume that the gas within the bubble behaves polytropically, such that

$$pV^{\kappa} = \text{constant}, \tag{1}$$

where p is the gas pressure within the bubble, of volume V, and where κ is the so-called polytropic index (which varies between γ, the ratio of the specific heat of the gas at constant pressure to that at constant volume, and unity, depending on whether the gas is behaving adiabatically, isothermally, or in some intermediate manner). Therefore the gas pressure and bubble volume at equilibrium (p_0, V_0) can be related to values at some general position through

$$\frac{p}{p_0} = \left(\frac{V_0}{V}\right)^{\kappa} = \left(\frac{A_0 x_0}{A_0 x_0 - A_0 \varepsilon}\right)^{\kappa} \tag{2}$$

where A_0 is the cross-sectional area of the bubble, ε the displacement of the meniscus from equilibrium, and x_0 the bubble length at equilibrium (see Figure 1). If $\varepsilon \ll x_0$ then equation (2) can be expanded to give the change in gas pressure from equilibrium to be

$$p - p_0 = \frac{\kappa \varepsilon p_0}{x_0}. \tag{3}$$

If an incremental displacement $\mathrm{d}\varepsilon$ occurs, and the bubble volume changes by $\mathrm{d}V = A_0 \mathrm{d}\varepsilon$, then the incremental change in the potential energy of the gas is

$$\mathrm{d}\Phi_{\mathrm{PE}} = -(p - p_0)\mathrm{d}V. \tag{4}$$

Integrating (4) from equilibrium to the extreme of the oscillation, ε_0, using substitution from (3), gives the maximum potential energy stored in the gas

$$\Phi_{\mathrm{PE,max}} = \int_0^{\varepsilon_0} \frac{\kappa A_0 p_0}{x_0} \varepsilon \mathrm{d}\varepsilon = \left(\frac{\kappa A_0 p_0}{x_0}\right) \frac{\varepsilon_0^2}{2}. \tag{5}$$

To calculate the kinetic energy of the liquid, assume the inertia of the gas to be negligible, owing to the much greater density (ρ) of the liquid. The total kinetic energy of the liquid is the sum of the kinetic energies of the liquid contained within the cone, and of the liquid column contained within the tube (Figure 1). Assume a harmonic displacement ε of the meniscus, $\varepsilon = \varepsilon_0 \mathrm{e}^{j\omega_0 t}$. Since the liquid is assumed to be incompressible, the kinetic energy of the liquid in the column (of equilibrium length $y_0 = H_1 - x_0$), of mass $\rho A_0 y_0$, occurs when the speed is a maximum (i.e. $|\dot{\varepsilon}_{\max}| = \omega_0 \varepsilon_0$) and the displacement zero, and equals

$$\Phi_{\mathrm{KE,max,col}} = \frac{1}{2} \rho A_0 y_0 \omega_0^2 \varepsilon_0^2. \tag{6}$$

Since the cross-sectional area in the cone increases with distance from the meniscus, the flow velocity of the incompressible liquid decreases in proportion. The area (A), radius (r) and distance from the imaginary apex of the cone (h) of a horizontal section through the cone are related to their values at the base of the column (A_0, r_0, and h_0 respectively -see Figure 1) through

$$\frac{A_0}{A} = \frac{\pi r_0^2}{\pi r^2} = \frac{\pi (h_0 \tan\theta)^2}{\pi (h \tan\theta)^2} = \frac{A_0}{\pi (h \tan\theta)^2} \tag{7}$$

where θ is the half-angle of the cone. The volume of liquid crossing all such areas A in a time $\mathrm{d}t$ must be constant if the liquid is incompressible, so that equating liquid fluxes gives the liquid velocity crossing the area A in the cone to be $\dot{\varepsilon}_0 A_0 / A$. Since $A \propto h^2$ (Eq. (7)), this gives an inverse-square law similar to that seen in spherically divergent geometries (see Discussion, Section 5). The volume of a

liquid element of thickness $\mathrm{d}h$ of cross-sectional area A in the cone is $\pi(h\tan\theta)^2\mathrm{d}h$; its mass is $\rho\pi(h\tan\theta)^2\mathrm{d}h$; and its maximum kinetic energy is

$$\frac{1}{2}\rho\pi(h\tan\theta)^2\mathrm{d}h|\dot{\varepsilon}_{\max}|^2(A_0/A)^2.$$

Substituting for A_0/A from (7), letting $|\dot{\varepsilon}_{\max}|$ equal $\omega_0\varepsilon_0$, and integrating up the kinetic energy of all the liquid elements in the cone gives the maximum kinetic energy of the liquid in the cone:

$$\begin{aligned}\phi_{\mathrm{KE,max,cone}} &= \\ &= \int_{h_0}^{H_2}\left(\frac{1}{2}\pi\rho(h\tan\theta)^2|\dot{\varepsilon}_{\max}|^2\left(\frac{A_0}{\pi(h\tan\theta)^2}\right)^2\right)\mathrm{d}h \\ &= \frac{1}{2}\frac{\rho(A_0\varepsilon_0\omega_0)^2}{\pi\tan^2\theta}\int_{h_0}^{H_2}\frac{\mathrm{d}h}{h^2} \\ &= \frac{1}{2}\frac{\rho(A_0\varepsilon_0\omega_0)^2}{\pi\tan^2\theta}\left(\frac{1}{h_0}-\frac{1}{H_2}\right). \end{aligned} \tag{8}$$

The total maximum kinetic energy of the incompressible liquid is therefore

$$\Phi_{\mathrm{KE,max}} = \Phi_{\mathrm{KE,max,col}} + \Phi_{\mathrm{KE,max,cone}}, \tag{9}$$

which can be found by substituting from (6) and (8):

$$\Phi_{\mathrm{KE,max}} = \frac{1}{2}\rho(\varepsilon_0\omega_0)^2A_0\left(y_0+\frac{A_0}{\pi\tan^2\theta}\left(\frac{1}{h_0}-\frac{1}{H_2}\right)\right). \tag{10}$$

The natural frequency of the undamped oscillator is found by equating $\Phi_{\mathrm{KE,max}}$ to $\Phi_{\mathrm{PE,max}}$, which can be done through equations (5) and (10), with appropriate inclusion of a term incorporating the effect of the viscosity of a liquid oscillating in a piston-like mode within a cylindrical confinement of radius r_0:

$$\omega_0 = \sqrt{\frac{\kappa p_0}{\rho x_0\left(y_0(1+\Lambda/r_0)+\dfrac{A_0}{\pi\tan^2\theta}\left(\dfrac{1}{h_0}-\dfrac{1}{H_2}\right)\right)}} \tag{11}$$

which is related to the linear natural frequency, f_0, through $\omega_0 = 2\pi f_0$. The boundary layer thickness is $\Lambda = (\mu/\pi\rho f_{\mathrm{p}})^{1/2}$, where μ is the liquid viscosity and f_{p} the linear resonance frequency of the piston-like mode resembling the one discussed in this paper (Miller & Nyborg, 1983).

Having found the natural frequency, the two key components of the oscillator, namely the inertia and the stiffness, can be examined in detail. The radiation mass m_r of this one-dimensional bubble can readily be found by noting that equation (10) must take the standard form $\Phi_{\mathrm{KE,max}} = m_{\mathrm{r}}|\omega_0\varepsilon_0|^2/2$ (Leighton, 1994). Therefore

$$\left.\begin{aligned} &m_{\mathrm{r}} = \rho A_0 y_0\left(1+\frac{A_0}{y_0\pi\tan^2\theta}\left(\frac{1}{h_0}-\frac{1}{H_2}\right)\right) \\ &\text{(inviscid liquids)} \\ &m_{\mathrm{r}} = \rho A_0 y_0\left((1+\Lambda/r_0)+\frac{A_0}{y_0\pi\tan^2\theta}\left(\frac{1}{h_0}-\frac{1}{H_2}\right)\right) \\ &\text{(viscous liquids).} \end{aligned}\right\} \tag{12}$$

The second term in the brackets incorporates the kinetic energy of the liquid in the cone. In inviscid conditions the first term (i.e. unity), which reflects the kinetic energy of the liquid in the column, is about two orders of magnitude greater than the second term. This is because whilst the liquid in the column has the same velocity as the meniscus, the liquid velocity in the cone falls off rapidly with depth (in the ratio A_0/A, i.e. as h^{-2}, as discussed after equation (7)). As a result the radiation mass of inviscid liquids is only about 1% greater than the mass of liquid in the column, $\rho A_0 y_0$. However the finite viscosity of water in the apparatus employed in this study (giving $\Lambda \approx 10^{-4}$ m) causes a $\sim$ 15% increase in the radiation mass. All these masses are very much less than the actual gravitational mass of liquid, which equals

$$\rho A_0 y_0\left(1+\frac{\pi\tan^2\theta}{3A_0y_0}(H_2^3-h_0^3)\right), \tag{13}$$

the first term (unity) representing the gravitational mass of the liquid in the column, and the second term (which for this apparatus is roughly two orders of magnitude larger) representing the gravitational mass of the liquid in the cone.

The stiffness k can be found by examining the force exerted by the bubble in response to a displacement ε. That force can be characterized through the change in gas pressure p, so that

$$k = A_0\frac{\partial p}{\partial\varepsilon}. \tag{14}$$

Differentiation of (2) provides $\partial p/\partial\varepsilon$. Substitution of this into equation (14) gives

$$k = \frac{\kappa p_0 A_0^2}{V_0}\left(1-\frac{A_0\varepsilon}{V_0}\right)^{-(\kappa+1)} \tag{15}$$

The stiffness is dependent on the displacement, and so will vary throughout the oscillatory cycle, increasing in compression, and decreasing in rarefaction. Figure 2 plots the stiffness of the gas for both positive and negative values of meniscus displacement ε. The nonlinear expression for stiffness, (15), is plotted as solid curves for both the adiabatic and isothermal limits. As can be seen from Figure 2, the stiffness increases in compression ($\varepsilon > 0$), and decreases in rarefaction. If the change in volume is so small as to be negligible compared to the equilibrium

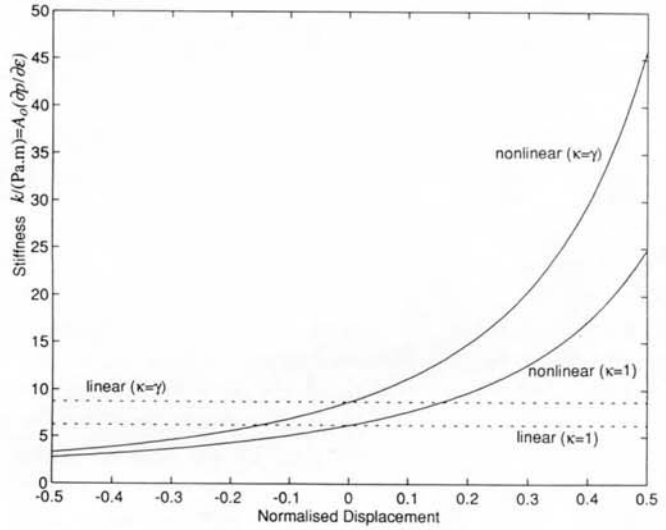

Figure 2. Plot of stiffness $k = A_0 \partial p / \partial \varepsilon$ in Pa m as a function of normalized displacement $(\varepsilon/\varepsilon_0)$ for air bubble in water. The apparatus used later in this study has $A_0 = 1.77 \times 10^{-6} \mathrm{m}^2$, and this value is used in the calculation. The bubble length chosen ($x_0 = V_0/A_0 = 65$ mm) is also typical of that which the apparatus can produce. The air pressure chosen was 10^5 Pa. Predictions in both the adiabatic ($\kappa = \gamma = 1.4$) and isothermal ($\kappa = 1$) limits are shown. Those from the nonlinear theory (i.e. from equation 15) are solid lines. The small amplitude approximate form (equation 16), which would predict linear oscillations, are broken lines.

bubble volume (i.e. $A_0\varepsilon \ll V_0$) then the stiffness becomes independent of displacement, and of value

$$k = \frac{\kappa p_0 A_0^2}{V_0}, \tag{16}$$

(as shown by the dashed plots in Figure 2). Therefore the natural frequency in the limit of small-amplitude oscillations is given by the root of the ratio of (16) to (12), giving equation (11) which, in the limit where the inertia of the liquid in the cone is neglected, reduces to

$$\omega_0 = 2\pi f_0 = \sqrt{\frac{\kappa p_0}{\rho x_0 y_0 (1 + \Lambda/r_0)}} \tag{17}$$

Within the approximations inherent in (17), the natural frequency is symmetrical about the midpoint of the column as regards the equilibrium position of the meniscus (solid plots in Figure 3a), ω_0 being a minimum when $x_0 y_0 = (H_1 - x_0)$ is a maximum (when $x_0 = y_0$). The resonance frequency becomes undefined for $y_0 \to 0$, as the bubble fills the column (and in the trivial case of no bubble present, i.e. $x_0 = 0$), a situation which is resolved when the mass of fluid outside the column (which now dominates the radiations mass) is reintroduced (dashed plots in Figure 3a, given by equation 11). The natural frequencies of tubes of various lengths which are filled by bubbles to 50%, 10%, 5% and 2% are shown in Figure 3b. Use of equation (17) is justified for tubes long in comparison with the bubble length and the tube diameter, when the inertia of the liquid outside the tube has negligible effect.

Equations (11) and (17) both employ an inherent assumption that the stiffness is independent of the displacement. Since the stiffness has in fact been shown to be displacement-dependent (equation 15), the actual response of the oscillator is found by incorporating this displacement-dependency, together with the radiation mass and damping, b, into the equation of motion:

$$\begin{aligned} & m_r \ddot{\varepsilon} + b\dot{\varepsilon} + k\varepsilon = F \Rightarrow \\ & \left(\rho A_0 y_0 \left((1 + \Lambda/r_0) + \frac{A_0}{y_0 \pi \tan^2\theta}\left(\frac{1}{h_0} - \frac{1}{H_2}\right)\right)\right)\ddot{\varepsilon} \\ & + b\dot{\varepsilon} + \frac{\kappa p_0 A_0^2}{V_0}\left(1 - \frac{A_0\varepsilon}{V_0}\right)^{-(\kappa+1)} \qquad \varepsilon = F \end{aligned} \tag{18}$$

Analytical phase space solutions can be found by expressing the undamped, unforced version ($b = 0$; $F = 0$) in terms of the normalized displacement $x = \varepsilon/x_0$ as

$$\ddot{x} + \omega_0^2 (1 - x)^{-(\kappa+1)} \quad x = 0 \tag{19}$$

where the constant ω_0^2 is defined by the formulation of (11). Note that whilst the notation ω_0^2 imitates the classical notation for the linear equation describing simple harmonic motion, in this nonlinear equation it only reflects the natural frequency for small displacements. Equation (19) can be solved in phase space by making the substitution

$$\ddot{x} = v\frac{\mathrm{d}v}{\mathrm{d}x} \quad \text{where } v = \dot{x} \tag{20}$$

to give the separable first order differential equation

$$v\frac{\mathrm{d}v}{\mathrm{d}x} = -\omega_0^2 (1 - x)^{-(\kappa+1)} x \tag{21}$$

Integration of both sides of this equation with respect to x yields

$$\left.\begin{aligned} v = \frac{\mathrm{d}x}{\mathrm{d}t} &= \omega_0 \sqrt{\frac{2(1 - \kappa x)}{\kappa(\kappa - 1)(1 - x)^{\kappa}} + c} \qquad (\kappa \neq 1) \\ v = \frac{\mathrm{d}x}{\mathrm{d}t} &= \omega_0 \sqrt{\frac{2}{(1 - x)} - \ln(1 - x) + c} \qquad (\kappa = 1) \end{aligned}\right\} \tag{22}$$

where c is an arbitrary constant. This equation relates displacement to velocity, that is, it is a solution in phase space. Further integration will be required to obtain displacement as an explicit function of time, a task best suited to numerical rather than analytical methods. However plotting the curves defined by (22) does enable the description of a trajectory of the solution in phase space.

Figure 4 illustrates four typical trajectories obtained from (22) for the free undamped oscillations of a bubble having $\omega_0/2\pi = 23$ Hz with four different initial displacements. The closed form of these curves indicates the periodic nature of the solutions. The curves are not of the ellipsoidal form that the linear model would produce, a

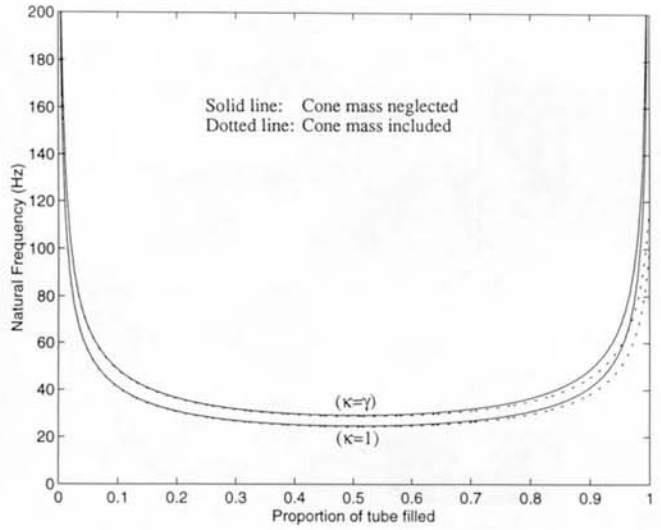

a)

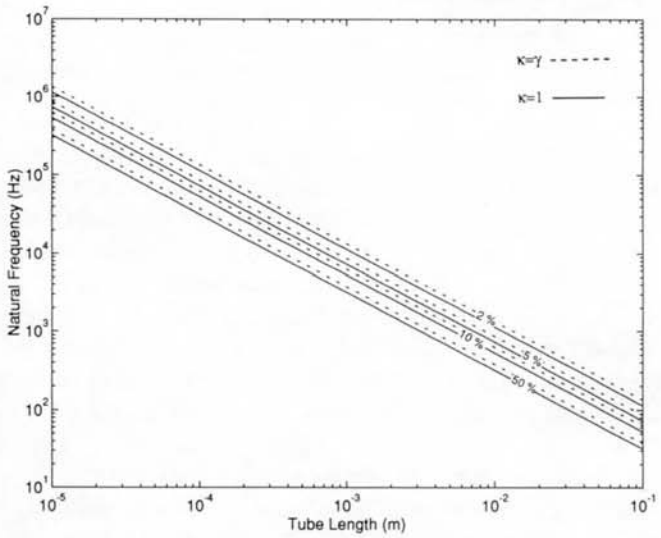

b)

Figure 3. a) Plots of the effect of bubble length, shown as a proportion of the tube length which is filled by air at equilibrium, on the natural frequency, as predicted by linear theory in the limit of small-amplitude oscillations. The tube length (H_1) and internal diameter (r_0) are set at 123 mm and 1.5 mm respectively, reflecting the dimensions of the experimental apparatus used in this study. The solid lines indicate calculations for which the inertia of the fluid in the cone is neglected, and the dashed lines correspond to calculations including the inertia of the fluid in the cone. The upper two plots correspond to the adiabatic ($\kappa = \gamma$) case, and the lower two to the isothermal ($\kappa = 1$) situation. Viscous effects are neglected. b) Plots of the effect of tube length on the natural frequency, for the adiabatic ($\kappa = \gamma$, broken lines) and isothermal ($\kappa = 1$, solid lines) cases. Results are shown for tubes filled at equilibrium by gas to a proportion (from the top) of 2%, 5%, 10% and, for the lowest lines, 50%. Tube diameter is assumed to be small compared to tube length, but surface tension and viscous effects are neglected.

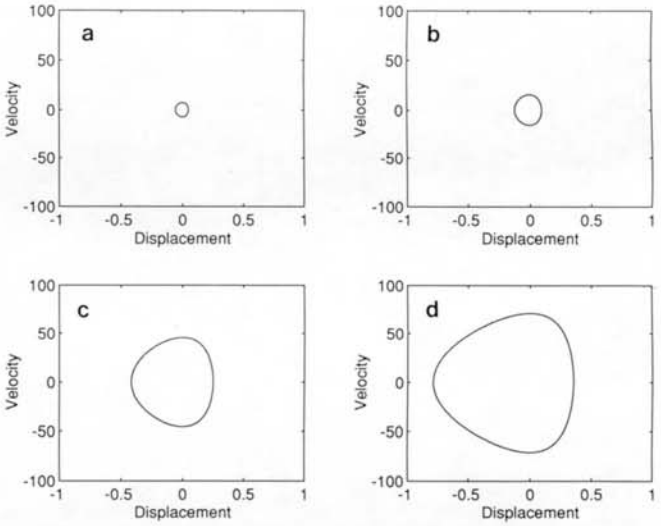

Figure 4. Solutions of equation (22) give phase space plots of bubble wall velocity as a function of wall displacement for the free undamped oscillation of a bubble having $\omega_0/2\pi = 23$ Hz. The normalized initial displacement increases from (a) to (d): (a) 0.05, (b) 0.10, (c) 0.25, (d) 0.35.

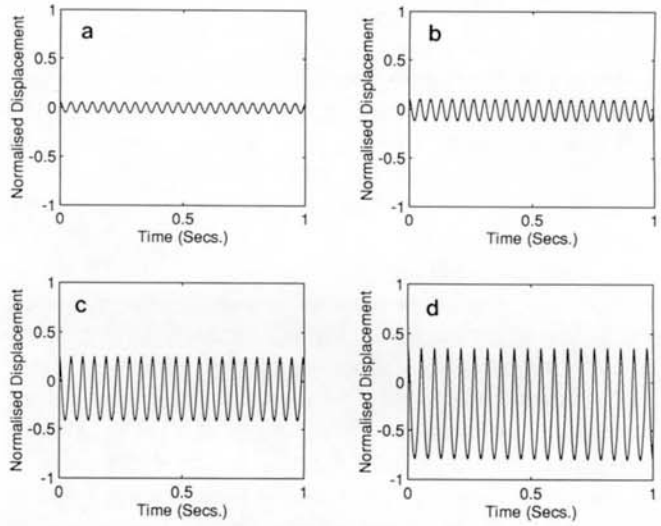

Figure 5. The displacement time histories associated with the solutions shown in the corresponding parts of Figure 4.

difference which increases with increasing initial displacement, indicating significant departures from linearity in these solutions.

Using numerical integration the time histories associated with the solutions shown in the corresponding parts of Figure 4 can be calculated (Figure 5). The corresponding frequency content of these solutions is shown in Figure 6. At small initial displacements the oscillation is nearly sinusoidal (Figure 5a), with a fundamental frequency of 23 Hz (Figure 6a), in accordance with the natural resonance predicted by the small-amplitude linear theory through equation (11). However for the larger initial displacements the greater the harmonic content of

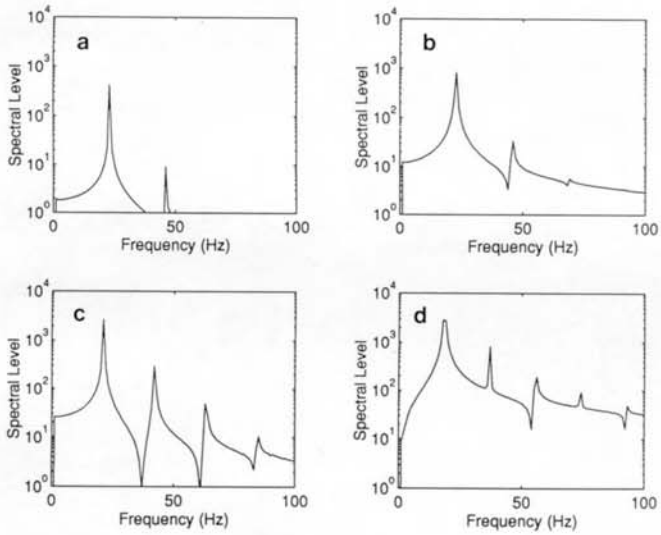

Figure 6. The frequency spectra associated with the displacement time histories shown in the corresponding parts of Figure 5.

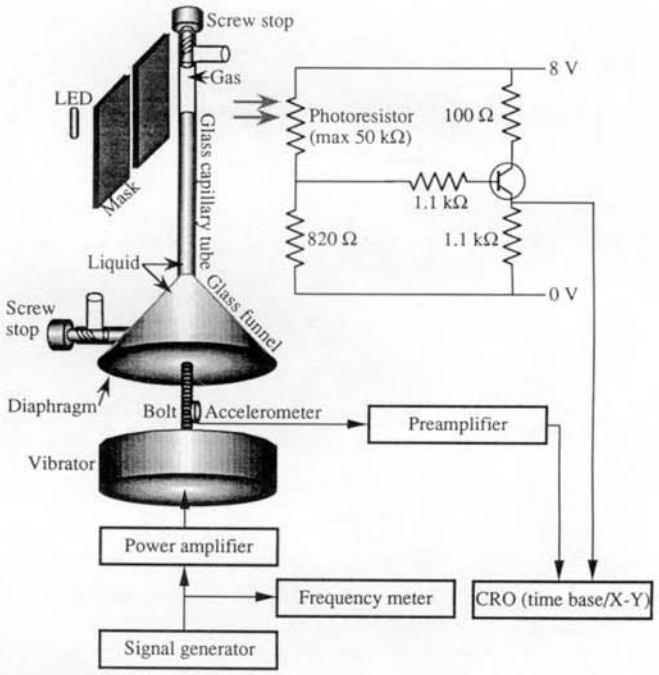

Figure 7. The apparatus employed to measure the phase response of a driven bubble.

the frequency spectrum (Figure 6), as reflected in the increasing asymmetry of the time histories in Figure 5. This arises because, in compression, the system has an increasing stiffness and therefore a more rapid response; conversely, in rarefaction, the stiffness is reduced and the response more sluggish, in agreement with Figure 2. The fundamental frequency, as given by the peak closest to the origin in each spectrum in Figure 6, decreases with increasing displacement, being (a) 23 Hz, (b) 23 Hz, (c) 21 Hz, and (d) 18 Hz.

The analytical treatment of the equations of motion which are either damped, forced, or both, is not feasible, and requires the adoption of the numerical path. The solution to (18) can be calculated using standard Runge-Kutta algorithms (Forsythe et al., 1977). A sinusoidal form for the forcing term is assumed. The size of the damping term can be obtained from theory, and has been solved for similar geometries, though the analysis is not simple (Miller & Nyborg, 1983; Miller & Neppiras, 1985). In this case estimates of the quality factor were obtained from experimental data (see later, Section 4), and a value of $Q = 3.5$ was chosen.

3. Experimental

An experimental one-dimensional model bubble was constructed within the laboratory in order to investigate the limitations of this theory. The bubble model uses glass capillary tubing of ≈ 123 mm length (depending on exact position of screw top), having an internal diameter of 1.5 mm and a wall thickness of about 2 mm, attached to an inverted glass funnel ($\theta = 30°$; $H_2 = 43.3$ mm). The base of this funnel is covered with a rubber diaphragm (Figure 7), which is connected by a bolt to the vibrator. Because of the area ratio of the funnel mouth to the diameter of the capillary tube, a small displacement of the diaphragm will produce a displacement approximately twenty times greater in the tube, so facilitating observation of the meniscus motion and minimizing vibration of the glassware. The glassware has two stopcocks attached at either end of the capillary to enable both the control of pressure and the introduction of a known amount of liquid (which was degassed, filtered, and colored with food dye).

The diaphragm is driven by a Ling vibrator (type 409) supplied by a sinusoidal signal, the excitation frequency and amplitude being made adjustable by the sinewave generator (Therlby Thandor type TG220) and amplifier. The acceleration is measured using an accelerometer connected *via* a charge amplifier (Bruel and Kjaer types 4367 and 2635 respectively) to a storage oscilloscope (Gould type OS1420).

Two types of measurements were made, each requiring a different set of equipment. The phase sensor comprised a photoresistor (NORP-12) and an LED which was masked to minimise light transmission through paths other than those which crossed the tube interior, such that the obscuration of the light by the dyed water produced a signal which, when incorporated into the circuit shown in Figure 7, could be used to monitor the meniscus displacement. The driver (accelerometer) and response (photoresistor) signals were displayed on the oscilloscope as an $X - Y$ plot, resulting in Lissajous figures. These could then be interpreted to give the driver-response phase relationship, once all the phase changes introduced by the electronics had been accounted for (including filter effects). The light detector signal was filtered to reduce

mains interference using a low pass filter (Barr and Stroud type EF3-04) set to 50 Hz. Since the accelerometer signal tended to be corrupted by noise, particularly at low frequencies and at low amplitudes, a 40 Hz low-pass filter (Fern Developments type EF5-02) was incorporated. The phase response for increasing frequencies was found for constant acceleration amplitude. Although adequate for the measurement of phase, this procedure proved to be inadequate for demonstrating an amplitude resonance. This was due to the fact that a constant amplitude voltage input signal to the vibrator, for increasing frequency, resulted in an increasing acceleration amplitude generated by the driver: hence to keep the acceleration amplitude constant (as monitored with the accelerometer), the input voltage to the vibrator had to be reduced each time the frequency was increased. This process decreases the displacement amplitude of the meniscus to such an extent that the optics used to measure displacements were not sensitive enough to detect a resonance peak. This problem was overcome by taking displacement measurements for constant input voltage to the driver as the frequency varied, the acceleration amplitude of the vibrator being continually recorded. The amplitude of displacement was found by illuminating the moving meniscus with a stroboscope (Dawe type 1204C) tuned to a frequency approximately twice that of the driver. This optically reduced the velocity of the image of the meniscus, so that the extreme of the oscillation could be measured using a travelling microscope (Type 2162-HB) with a Vernier scale.

4. Results

The experimental results, taken at discrete frequencies, demonstrate the phase relationship between the driver and one bubble (Figure 8), and the amplitude response of another bubble (Figure 9), as a function of frequency. Table 1 summarizes the experimental parameters and resonance frequencies, as determined from these experimental data, and as calculated (for $\kappa = 1$ and $\kappa = \gamma$) from small-amplitude linear theory (equation 11), and through the numerical solution of (18). The results of these integrations, which allow for finite amplitude nonlinear damped oscillations and employ the experimentally-determined quality factor of 3.5, are shown in Figures 8 and 9 as dotted plots for $\kappa = 1$ and $\kappa = \gamma$, (labelled "with viscosity"). To demonstrate the importance of viscosity (an effect which is often of secondary importance for spherical bubbles - Minnaert, 1933), dashed lines (labelled "inviscid") in Figures 8 and 9 show the results of setting μ to zero in equation (18). Table 1 includes these numerical predictions of the resonance found through inviscid nonlinear theory, as well as the estimations of linear inviscid theory found by setting $\mu = 0$ in equation (11).

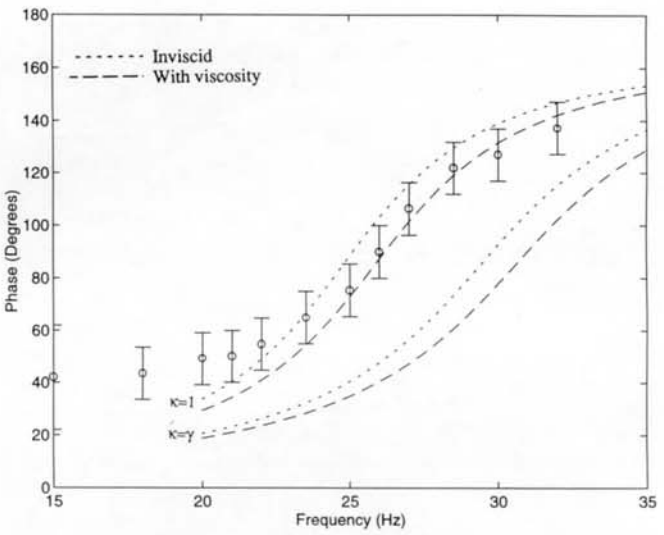

Figure 8. The phase response of the driven bubble ($x_0 = 71.5 \pm 0.5$ mm, $y_0 = 52.0 \pm 0.5$ mm). Vibrator acceleration amplitude: 8.92 m/s^2. Experimental measurements are taken at discrete frequencies. The numerical solutions are shown for the adiabatic ($\kappa = \gamma$) and isothermal ($\kappa = 1$) cases, as the labels show. Solutions are shown for the equation of motion (18) incorporating both viscous effects (short dashes, - - - -) and for the inviscid case (long dashes, – – –).

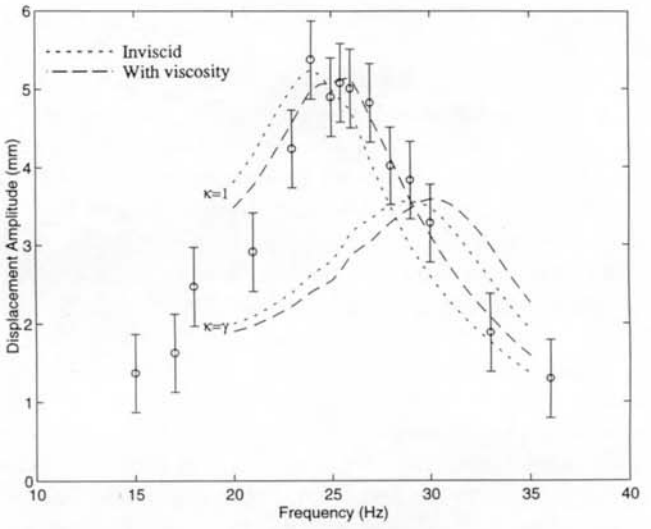

Figure 9. The amplitude response of the driven bubble ($x_0 = 70.0 \pm 0.5$ mm, $y_0 = 53.0 \pm 0.5$ mm), driven with a vibrator acceleration amplitude which increases linearly with frequency from 9 m/s^2 at 15 Hz to 45 m/s^2 at 36 Hz. Experimental measurements are taken at discrete frequencies. The numerical solutions are shown for the adiabatic ($\kappa = \gamma$) and isothermal ($\kappa = 1$) cases, as the labels show. Solutions are shown for the equation of motion (18) incorporating both viscous effects (short dashes, - - - -) and for the inviscid case (long dashes, – – –).

Table 1. *Comparison of the experimentally-determined resonances with those determined by piston-mode theory: linear (equation 11) and numerical (equation 18), for* $p_0 = 10^5$ *Pa,* $\mu = 10^{-3}$ *Pa and* $\rho = 1000$ *kg* m^{-3}. *Bubble size and vibrator acceleration are indicated.*

Fig	$\frac{x_0}{\text{mm}}$	$\frac{y_0}{\text{mm}}$	Vibrator acceleration amplitude /(s^{-2}m)	Resonance (Linear viscous theory, eq. 11) /(Hz)	Resonance (Numerical viscous theory, eq. 18)/(Hz)	Resonance (Linear inviscid theory, eq. 11, $\mu = 0$)/(Hz)	Resonance (Numerical inviscid theory, eq. 18, $\mu = 0$) /(Hz)	Resonance (Experimental) /(Hz)
8	71.5 ± 0.5	52.0 ± 0.5	8.92	24.1 ± 0.2 ($\kappa = 1$) 28.8 ± 0.2 ($\kappa = 1.4$)	25.0 ± 0.5 ($\kappa = 1$) 30.0 ± 0.5 ($\kappa = 1.4$)	26.1 ± 0.2 ($\kappa = 1$) 30.9 ± 0.2 ($\kappa = 1.4$)	26 ± 0.5 ($\kappa = 1$) 31 ± 0.5 ($\kappa = 1.4$)	26 ± 1
9	70.0 ± 0.5	53.0 ± 0.5	See Figure 9 caption	24.4 ± 0.2 ($\kappa = 1$) 28.8 ± 0.2 ($\kappa = 1.4$)	24.0 ± 0.5 ($\kappa = 1$) 29 ± 1 ($\kappa = 1.4$)	26.1 ± 0.2 ($\kappa = 1$) 30.8 ± 0.2 ($\kappa = 1.4$)	26 ± 1 ($\kappa = 1$) 30 ± 1 ($\kappa = 1.4$)	26 ± 2

5. Discussion

Recalling that experimental results should lie at frequencies on or between the pair of curves which, for a given assumed viscosity, correspond to the limits of $\kappa = 1$ and $\kappa = \gamma$, Figures 3 and 4 indicate that the viscous theory fits best, and that the conditions are closer to the isothermal than the adiabatic. This is supported in Table 1, best agreement with experiment occurring when viscosity is incorporated into the theory. The simple linear theory gives adequate predictions of the resonance, even when the inertia of the liquid within the cone is neglected, as expected when the column contains a significant amount of water.

The theory contains assumptions that should be outlined. The acceleration is assumed to be uniform over the diaphragm, which it is not clearly since in the experimental bubble the perimeter is fixed. Also the effects of friction, and surface tension have been neglected. Whilst deformations of the meniscus have been neglected, such deformations are however readily observable in the experimental bubble, and are of an oscillatory nature. The presence of a second oscillation in the system may clearly have important implications on the dynamics.

The dynamics of similar oscillators have been studied in the past. Howkins (1965) made observations and preliminary calculations regarding the oscillations of gas bubbles in water attached to the submerged base of an inverted vibrator (both roughly spherical bubbles beneath a plane face, and gas pockets trapped within "pits" within the base). Analyses have been made of several other cases. Miller (1979) studied cylindrical bubbles bounded by elastic walls, to model the response to ultrasound of gas spaces of micron-order size between plant cells within *Elodea*. The cylindrical bubbles within this model were assumed to vibrate in the radial mode, rather than be dominated by motion of the end-walls, and the stiffness of the plant walls was dominant over the stiffness of the gas. Other analyses include the diaphragm-like oscillation of the meniscus as it undergoes a Bessel-function deformation, the so-called "clamped-drumhead" vibration. This was first considered for a small circular meniscus within a solid plane (i.e. having infinitesimal thickness, but infinite in the other two dimensions) separating two half-spaces, one of gas and the other, liquid (Miller, 1979). The oscillator was therefore baffled, as were two later geometries in which this membrane was placed: a gas pocket fully filling first a uniform perforation through, and second a uniform circular pit within, a submerged solid sheet (Miller & Nyborg, 1983). In all these cases the resonance frequency and the damping were found. The "clamped-drumhead" resonance of a meniscus within a partially-filled perforation and pit within a flat solid sheet was also found. This case represented a departure from the earlier ones, in that the inertia was not solely invested in the liquid outside the hole, but also included that due to the liquid in the hole. Miller & Nyborg (1983) also examined the piston-like motion of the bubble wall, as discussed in this paper, but only for the baffled case, where the gas fully fills the pore. This constraint was relaxed somewhat by Miller & Neppiras (1985), who discussed the oscillations of partially-filled pores within a flat solid sheet in terms of two distinct regimes, those of "clamped-drumhead", and of piston-like, motion. At small amplitudes, symmetrical perforations gave the same resonances as pits which had the same depth and gas content as half of a perforation. Exploiting this fact to adopt the notation employed in this paper, the circular resonance frequency ω_m of the clamped-drumhead model of a bubble in a baffled perforation or pit would be:

$$\omega_m = 2\pi f_m = \sqrt{\frac{120\pi\sigma x_0 + 15\kappa p_0 A_0}{32\rho x_0 r_0^3 + 15 A_0 \rho x_0 y_0 (1 + \Lambda/r_0)}} \quad (23)$$

where σ is the surface tension.

One-dimensional bubbles of interest exist in biological structures, and some of these are exposed to intense sound of a particular frequency. Two examples are discussed here. The first case is of one-dimensional bubbles

trapped within ear canals of divers, and the adverse effects on divers and other mammals exposed to high intensity sound in the marine environment is currently of great concern. The second case is of one dimensional bubbles trapped within a capillary blood vessel. This may occur particularly in the lung, and evidence suggests that the lowest thresholds for damage by clinical ultrasound in mammals *in vivo* are found in the lung.

Divers today are increasingly becoming exposed to high-powered sound in the underwater environment both as unwanted noise from apparatus associated with their work, and from the increasingly common acoustic techniques associated with communication, exploration, monitoring, and exploitation of the oceans by man. Apparatus may include tools operated by the divers themselves (including stud guns, plasma cutters, rock drills, jet cleaning tools, impact wrenches, grinders and drills) which may produce sound pressure levels (SPL) of 150-170 dB (re 20 μPa) underwater, up to 210 dB (re 20 μPa) having been recorded (Molvaer & Gjestland, 1981; Nedwell et al., 1993). Tool emissions occur over a wide frequency range, at least from a few 10 Hz to around 10 kHz (Nedwell et al., 1993). Whilst active sonar operates from a few kHz up to around 100 kHz, given the dimensions of the ear canal (Davis, 1978) of particular interest are experiments involving the propagation of low frequency sound (from a few tens of Hz up to a few hundred) over long ranges (of order 1000 km) for climate monitoring. For detection over such long ranges, the sources of such sound are necessarily powerful (220 dB re 1 μPa at 1 m; Baggeroer & Munk, 1992).

Comparatively little is known about air bubbles trapped within the ear canals of submerged humans. These bubbles are capable of having a significant effect on underwater hearing (Al Masri, 1993). The geometry of these bubbles is not known, but the most likely shape is a cylindrical gas pocket, bounded at the curved wall by the flesh of the ear canal itself, and at the ends by the ear drum and the gas/water interface within the ear canal. The remainder of the canal would be water filled leading to the pinna, where a much larger body of water occurs external to the head. As with the column-cone model of the liquid body used in this investigation, the inertia of the oscillator will be invested primarily in the liquid contained within the ear canal, the radiation mass associated with the water outside of the head being far less significant, and the inertia of the entrained gas within the ear negligible. Therefore use of the simple linear theory given by equation (17) is justified for making estimations of the resonances (though clearly there is elasticity associated with the fleshy boundaries). Given typical ear canal dimensions, simple linear theory predicts that air bubbles trapped within divers' ears may be expected to resonate at frequencies as shown in Figure 10. The resonances for the clamped-diaphragm model (equation 23) are also shown. Because of the relative gas volume changes which the two geometries can generate,

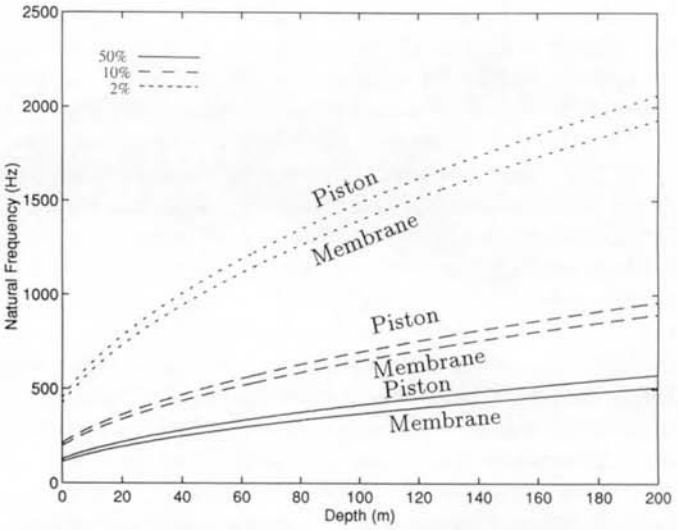

Figure 10. Resonance of air bubbles in ear canals as a function of depth h (acting through ρgh) for a 2.5 cm ear canal of diameter 5 mm filled to (a) 50% (solid line —), and (b) 10% (dashed – – –) and (c) 2% (dotted line - - - -). The piston-like modes (equation 17) and membrane-like modes (equation 23) are labelled, and isothermal oscillations ($\kappa = 1$) are assumed. Viscosity is incorporated, but the inertia of the liquid outside the canal is neglected (justified since the filling of air is to less than 50%). Values of 72 mN/m, 1000 kg/m^3 and 9.8 m/s^2 are assumed for the (fresh) water surface tension (σ), density (ρ) and acceleration due to gravity (g), respectively.

it is likely that the piston-like motion can generate the larger pressure fluctuations within the gas. The energetics of such resonances, and their harmonics (of the type illustrated in Figure 6), clearly may cause a noticeable effect within a system which is designed to be sensitive to acoustic stimulation through gas, rather than liquid, adjacent to the eardrum. The mechanisms of underwater hearing itself are involved (Al Masri, 1993) and it is not a simple matter to theoretically extrapolate from this to predict the effect of such bubbles on underwater hearing. However human diving is potentially hazardous, and the occurrence of any resonances coupling the human hearing, orientation and balance systems to an ocean medium which can contain intense sound at those frequencies must be considered.

There is far more documented evidence concerning the situations where one-dimensional bubbles might be expected to be exposed to high intensity ultrasonic fields. The excitation of gas pockets which are stabilized within biological structures, the so-called "gas body activation" (Miller, 1984) was first considered to interpret the biological effects of ultrasound on the leaves of the aquatic plant *Elodea*, as discussed earlier (Miller, 1977). Such bodies have also been considered to discuss the mechanism of bioeffect when pockets of gas trapped in blood vessels, insect trachae and mammalian cells are subjected to ultrasonic irradiation.

There are conceivably many mechanisms of acoustic interaction with matter through which ultrasound could generate a bioeffect (ter Haar, 1986), and these potentially include both cavitational and non-cavitational ones. The relative effectiveness of these will depend on the specific conditions which exist, including those relating to the incident sound field (e.g. frequency, amplitude, pulsing characteristics, focusing) and those relevant to the medium (e.g. ultrasonic absorption, the presence of bones, perfusion etc.). The critical importance of the availability of cavitation nuclei has been recognized for several decades. The combination of these features determines the activities through which cavitational bioeffects may potentially arise. If driven at low amplitude, the bubble will oscillate stably and repeatably, and such stable cavitation (of spherical bubbles) has been observed to cause bioeffect. Mechanisms involving stable cavitation include firstly those effects associated simply with the formation of stable bubbles (through rectified diffusion, the effect of ultrasonically-induced temperature rises on gas solubility and vapour pressure), which may bring about decompression-type symptoms. Other potential mechanisms for bioeffect are associated with the motions, either oscillatory or rectilinear, of stable spherical bubbles, including microstreaming and effects related to radiation forces generating high-speed bubble translations, particle aggregations etc. Of particular concern has been the phenomenon of "unstable" or "transient" cavitation, typified by the explosive growth of unconfined spherical bubbles, followed by their rapid collapse. This collapse typically involves gas shocks and adiabatic heating of the gas to high temperature, both processes being capable of generating free radicals. The collapse is followed by a rebound, capable of generating liquid shocks. Though the field has been dominated by models of spherical bubbles (Leighton, 1994; Holland & Apfel, 1989; Apfel & Holland, 1991) cylindrical bubbles may also show the equivalent of "stable" and "transient" regimes[2].

Microstreaming from stable cavitation can cause cell death in *Elodea* (Miller, 1985). Vivino et al. (1985) demonstrated similar results using Nuclepore^{TM} to induce cell lysis in spleen cells *in vitro* at a spatial peak threshold intensity in excess of 75 mW cm^{-2}, at an acoustic frequency of 1.6 MHz continuous-wave. These experiments, using Nuclepore^{TM}, are characterized by the very low intensities at which bioeffects can be detected: Williams & Miller (1980) used photometry to detect ATP release from *in vitro* human erythrocytes, a technique which has probably produced effects at the lowest continuous-wave intensity recorded for a detectable bioeffect, 4 mW cm^{-2} (Williams, 1983). The mechanism was probably rupture or a change in permeability of the cell membrane brought about through microstreaming stresses at the cell wall. Other effects reported with this technique include platelet aggregation (Miller et al., 1979) and hemolysis (Miller, 1988; Miller & Thomas, 1990). In an examination of mechanisms in the latter process, Miller & Thomas (1990) suggest that the increased hemolysis observed at elevated ambient temperatures is a result of the reduced viscosity, and consequently modified liquid flow near the cell, rather than increased cell fragility.

In addition to "stable cavitation" of cylindrical bubbles, a "transient" regime[2] also exists. However if the gas bodies stabilized within biological structures resemble the one-dimensional bubbles discussed earlier in this paper, in certain circumstances it would be expected that the growth phase is the key mechanism for bioeffect, in contrast to the traditional emphasis on the collapse phase in the transient cavitation of spherical bubbles. If the medium resists bubble growth (for example, it is a liquid constrained to a fixed volume by structure, such as a mammalian cell; or the gas pocket is itself part-bounded by rigid walls, for example the larval trachae), then stresses can be induced by the growth which may damage the restraining structure (Ward et al., 1983; Venter et al., 1983; Aymé & Carstensen, 1989a). Child et al. (1981) suggested that larval gas pockets might be used to model the response of bubbles within mammalian cells, particularly in respect to μs diagnostic-type pulses. Whereas in the plant tissues studies it had been found that the stiffness of the walls contributed significantly to the dynamics, preliminary low-level continuous-wave studies had shown that the walls of the insect tracheae do not contribute significantly to the dynamics of larval gas pockets, and model the case of human tissues more closely. Child et al. (1981) demonstrated the susceptibility of fruit fly larvae (Drosophilia melanogaster) to diagnostic-type insonation (with pulse length of 1 μs, giving a low time-averaged acoustic intensity), with a sharp threshold (around 1 MPa in a 2.5 min exposure). Evidence, including the coincidence of the killing and transient cavitation thresholds (Flynn, 1982; Child et al., 1981), suggests a cavitation-type mechanism on the larvae (Child & Carstensen, 1982; Berg et al., 1983; Carstensen et al., 1983a; Carstensen et al., 1983b), probably acting primarily through these micrometer-sized gas bodies within the organisms (Child & Carstensen, 1982). The effect was related to temporal peak, rather than the temporal average, intensity, a characteristic of the rapid response found in transient cavitation.

These results are further interpreted in the light of subsequent results in the field of extracorporeal shock wave lithotripters. Damage resulting from such exposure *in vivo* often manifests in vessel walls, particularly in capillaries and medium-sized veins, with focal lesions in arterial walls tending to occur much less frequently (ter Haar et al., 1994; Delius et al. 1990a and b).The most sensitive organ to shock wave exposure is the lung. Hartman et al.

[2]The equivalence is not rigorous. It does not extend to the well-defined phenomenon of inertial cavitation, but only bears similarities with the initial explosive growth associated with the less well-defined phenomenon of transient cavitation.

(1990a and b) found that comparatively mild lithotriptic exposures were required to haemorrhage mouse lung (less than 2 MPa for only 10 pulses). Severe damage occurred at 5 to 6 MPa. In contrast fetal lung did not show damage at 20 MPa. This is presumed to be because of the absence of stabilized gas bodies within the fetal lung (ter Haar et al., 1994). Noting that Child et al. (1990) and Frizzell et al. (1994) have observed haemorrhage in mammalian lung resulting from exposure to pulsed ultrasound at levels low compared to those required to produce cavitation in tissues that do not contain stabilized gas bodies, ter Haar et al. (1994) comment that whilst the mechanism is not clear, it does appear to be mediated by existing stabilized gas bodies in tissue.

The hypothesis is that one-dimensional bubbles within lung capillaries may rupture the capillary during their growth phase. Clearly the considerations pertinent to the transient cavitation of spherical bubbles and the mechanical index (e.g. a suitable free-floating microscopic spherical nucleus - Holland & Apfel, 1989; Apfel & Holland, 1991) are inappropriate if the dynamics involved are those of a macroscopic cylindrical gas pocket trapped within such a blood vessel. Such pockets might arise dynamically, for example by the ultrasonically induced growth of a nucleus to a diameter similar to that of the capillary. Stable pockets can also become trapped as they flow through ever-narrowing vessels (de Jong et al, 1991, 1993; Schneider et al., 1992). Conditions within the blood flowing from the heart to the lungs are designed to encourage gas to come out of solution. Whilst gas may transfer directly from the blood into the capillary wall, to the air-vesicle wall and from thence to the air space, the conditions are such that gas may come out of solution within the blood itself (indeed, the interface between the blood and the vessel wall provides a suitable location for the nucleation of exsolution). This condition might also arise were gas-filled echo-contrast agents to migrate to blood vessels comparable with their size.

The response of the one-dimensional bubble from this moment becomes radically different from that of the free-floating spherical bubbles normally considered, since the inertial term does not asymptotically tend to a finite value unless the enclosing tube widens significantly. For a pulsating spherical bubble of equilibrium radius R_0, the radiation mass has value $4\pi R_0^3 \rho$ (Leighton, 1994). This has a finite and relatively small value because of the diverging geometry: if the meniscus velocity is $\dot{R}$ when the bubble has an instantaneous radius of R, then because of the spherically diverging geometry the liquid particle velocity at a distance r from the bubble centre is $\dot{r} = \dot{R}\,(R^2/r^2)$ (Minnaert, 1933). This inverse square law means that at large distances from the bubble, the liquid velocity is very small, so that the total kinetic energy invested in the liquid is finite, even within an infinite liquid medium. In contrast the liquid geometry in the one-dimensional bubble system shown in Figure 1 clearly does not begin to diverge until the cone section, the inertial contribution from the liquid contained within the glass capillary tube increasing monotonically with the tube length. This can also been seen by examining the two contributing terms to the radiation mass for this system as given in equation (12): the inertia of the liquid in the pipe is $\rho A_0 y_0$ in the inviscid case, and $\rho A_0 y_0 (1 + \Lambda/r_0)$ for viscous liquids, and within an infinite non-diverging pipe the bubble would have infinite inertia, and so not be an oscillator at all. On expansion within the blood system, for example after the passage of a compressive pressure pulse or under a tension, the one-dimensional bubble cannot move the massive column of liquid, and stresses will be exerted on the capillary wall and the meniscus. If the stresses so exerted within the capillary wall are greater than the cohesion between the single layer of cells which make up the blood vessel wall, then haemorrhage will occur. The only other "give" in the expanding one-dimensional bubble within the blood vessel is the meniscus: this will bow, causing local fluid motion and in the first instance, small gas volume change. If the deformation is sufficiently extreme daughter bubbles will be generated. However to do this a uniformly-bowing meniscus must pass through the hemispherical condition, where the surface tension pressure is a maximum. For a typical capillary of diameter $\approx$ 10 μm this corresponds to a confining pressure of $\approx$ 23 kPa. Adhesion between capillary cells must exceed this to prevent haemorrhage. The ultimate tensile strength of the weakest tissue noted by Yamada (1973) is 50 kPa. Should daughter bubbles be (in fact) produced, these may seed further expansions, though still confined by the capillary. In summary, the geometry acts against allowing the large-scale gas expansion required to relieve the stress on the capillary wall, and so prevent haemorrhage.

6. Conclusions

The dynamics of a one-dimensional bubble have been developed, including a simple analysis of small-amplitude linear oscillations, analytical phase-space solutions of the undamped unforced equation of motion, and numerical solution to the full equation of motion, in agreement with the oscillations of a laboratory bubble of centimeter-order length. With one-dimensional bubbles of such size, viscous effects are not negligible. The physical insights gained by the models allowed examination of two potentially biologically-significant cases. First, the bubble is adjacent to the ear drum, and acts as an oscillator which resonates at the low frequencies of the same order as the underwater sound which is becoming increasingly common in the ocean at high amplitude, both as noise from tools and for use in scientific investigation of the oceans. Second, bubbles in pipes are subject to pressure pulses and at some stage in their growth have a diameter similar to that of the pipe, which is itself very much longer than this dimension. The pipe system prevents geometrical spreading of the liquid, which consequently has very

large inertia. As a result significant stresses may be exerted on the pipe wall, potentially causing rupture. The application of this second case to the ultrasonic exposure of mammalian lung capillaries is discussed.

Acknowledgements

TGL wishes to thank the EPSRC (GR/H 79815) for funding, and D.G. Ramble and A.D. Phelps for assistance.

References

AL MASRI M.A.O. (1993) "Underwater Hearing Thresholds and Hearing Mechanisms", University of Southampton, Ph.D. Thesis

APFEL R.E., HOLLAND C.K. (1991) "Gauging the likelihood of cavitation from short-pulse, low-duty cycle diagnostic ultrasound", Ultrasound Med. Biol., 17, 179-185

AYMÉ E.J., CARSTENSEN E.L. (1989) "Cavitation induced by asymmetric distorted pulses of ultrasound: Theoretical Predictions", IEEE Trans. Ultrasonics, Ferroelectrics and Frequency Control, 36, 32-40

BAGGEROER A., MUNK W. (1992) "The Heard Island Feasibility Test", Phys. Today, 45, 22-30

BERG R.B., CHILD S.Z., CARSTENSEN E.L. (1983) "The influence of carrier frequency on the killing of drosophilia larvae by microsecond pulses of ultrasound", Ultrasound Med. Biol., 8, L448-L451

CARSTENSEN E.L., CHILD S.Z., LAM S., MILLER D.L., NYBORG W.L. (1983a) "Ultrasonic gas-body activation in *Drosophilia*", Ultrasound Med. Biol., 9, 473-477

CARSTENSEN E.L., BERG R.B., CHILD S.Z. (1983b) "Pulse average vs. maximum intensity", Ultrasound Med. Biol., 9, L451-L455.

CHILD S.Z., CARSTENSEN E.L., LAM S.K. (1981) "Effects of ultrasound on *Drosophila*-III. Exposure of larvae to low-temporal-average-intensity, pulsed irradiation", Ultrasound Med. Biol., 7, 167-173

CHILD S.Z., CARSTENSEN E.L. (1982) "Effects of ultrasound on *Drosophila*-IV. Pulsed exposures of eggs", Ultrasound Med. Biol., 8, 311-312

CHILD S.Z., HARTMAN C.L., SCHERY L.A., CARSTENSEN E.L. (1990) "Lung damage from exposure to pulsed ultrasound", Ultrasound Med. Biol., 16, 817

DAVIS H. (1978) "Hearing and Deafness", Davis H. and Silverman S.R., ©1947 Holt, Rinehart and Winston (New York, London), 4th Edition, Chapter 3 "Anatomy and Physiology of the Auditory System"

DELIUS M., JORDAN M., LIEBICH H.-G., BRENDEL W. (1990a) "Biological effects of shock waves: Effect of shock waves on the liver and gallbladder wall of dogs - Administration rate dependence", Ultrasound Med. Biol., 16, 459-466

DELIUS M., DENK R., BERDING C., LIEBICH H., JORDAN M., BRENDEL W. (1990b) "Biological effects of shock waves: cavitation by shock wave in piglet liver", Ultrasound Med. Biol., 16, 467-472

FLYNN H.G. (1982) "Generation of transient cavities in liquids by microsecond pulses of ultrasound", J. Acoust. Soc. Am., 72, 1926-2932

FORSYTHE G.E., MALCOM M.A., MOLER L.B. (1977) "Computer Methods for Mathematical Computations", Prentice-Hall.

FRIZZELL L.A., CHEN E., LEE C. (1994) "Effects of pulsed ultrasound on the mouse neonate: hind limb paralysis and lung haemorrhage", Ultrasound Med. Biol., 20, 53-63

HARTMAN C., COX C.A., BREWER L., CHILD S.Z., COX C.F., CARSTENSEN E.L. (1990a) "Effects of lithotripter fields on development of chick embryos", Ultrasound Med. Biol., 16, 581-585

HARTMAN C., CHILD S.Z., MAYER R., SCHENK E., CARSTENSEN, E.L. (1990b) "Lung damage from exposure to the fields of an electrohydraulic lithotripter", Ultrasound Med. Biol., 16, 675-679

HOLLAND C.K., APFEL R.E. (1989) "An improved theory for the prediction of microcavitation thresholds", IEEE Trans. Ultrason. Ferroelectrics and Frequency control, 36, 204-208

HOWKINS S.D. (1965) "Measurements of the resonant frequency of a bubble near a rigid boundary", J. Acoust. Soc. Am., 37, 504-508

DE JONG N., TEN CATE F.J., LANCÉE T.C., ROELANDT J.R.T.C., BOM N. (1991) "Principles and recent developments in ultrasound contrast agents", Ultrasonics, 29, 324-330

DE JONG N., TEN CATE F.J., VLETTER W.B., ROELANDT J.R.T.C. (1993) "Quantification of transpulmonary echocontrast effects", Ultrasound Med. Biol., 19, 279-288

LEIGHTON T.G. (1994) "The Acoustic Bubble", Academic Press, London

MILLER D.L. (1977) "The effects of ultrasonic activation of gas bodies in *Elodea* leaves during continuous and pulsed irradiation at 1 MHz", Ultrasound in Med. Biol., 3, 221-240

MILLER D.L. (1979) "A cylindrical bubble model for the response of plant-tissue gas-bodies to ultrasound", J. Acoust. Soc. Am., 65, 1313-1321

MILLER D.L., NYBORG W.L., WHITCOMB C.C. (1979) "Platelet aggregation induced by ultrasound under specialized condition *in vitro*", Science, 205, 505

MILLER D.L., NYBORG W.L. (1983) "Theoretical explanation of the response of gas-filled micropores and cavitation nuclei to ultrasound", J. Acoust. Soc. Am., 73, 1537-1544

MILLER D.L. (1984) "Gas body activation", Ultrasonics, 22, 261-269

MILLER D.L. (1985) "Microsteaming as a mechanism of cell death in *Elodea* leaves exposed to ultrasound", Ultrasound Med. Biol., 11, 285-292

MILLER D.L., NEPPIRAS E.A. (1985) "On the oscillation mode of gas-filled micropores.", J. Acoust. Soc. Am., 77, 946-953

MILLER D.L. (1988) "The influence of hematocrit on hemolysis by ultrasonically activated gas-filled micropores", Ultrasound Med. Biol., 14, 293-297

MILLER D.L., THOMAS R.M. (1990) "The influence of variations in biophysical conditions on hemolysis near ultrasonically activated gas-filled micropores", J. Acoust. Soc. Am., 87, 2225-2230

MINNAERT M. (1933) "On musical air-bubbles and sounds of running water", Philos. Mag., 16, 235-248

MOLVAER O.I., GJESTLAND T. (1981) "Hearing damage risk to divers operating noisy tools underwater", Scan. J. Work Environ. Health, 7, 263-270

NEDWELL J.R., MARTIN A.M., MANSFIELD N. (1993) "Underwater tool noise: Implications for hearing loss." In: Advances in Underwater Technology, Ocean Science and Offshore Engineering. Society for Underwater Technology, Kluwer Academic Publishers, Netherlands, 31, 267-275

SCHNEIDER M., BUSSAT P., BARRAU M.-B. et al. (1992) "Polymeric microballoons as ultrasound contrast agents. Physical and ultrasonic properties compared with sonicated albumin.", Investigat. Radiol., 27, 134-139

TER HAAR G., FRIZZELL L.A., DELIUS M., STRATMEYER M. (1994) "Non-thermal bio-effects: Organs, Cells, Tissues". WFUMB Symposium on Safety of Ultrasound in Medicine: Emphasis on non-thermal mechanisms (Draft Document, Utsunomiya, Japan, 11-15 July) Chapter 5

TER HAAR G.R. (1986) "Therapeutic and surgical applications." In: Physical principles of Medical Ultrasonics. CR Hill Ed., Ellis Harwood Ltd, Chichester (for John Wiley and Sons, New York). Part III: Biophysical implications and applications

VENTER R.D., WARD C.A., HO S., JOHNSON W.R., FRASER W.D., LANDOLT J.P. (1983) "Fracture studies on mammalian semicircular canal", Undersea Biomed. Res., 10, 225-240

VIVINO A.A., BORAKER D.K., MILLER D., NYBORG W. (1985) "Stable cavitation at low ultrasonic intensities induces cell death and inhibits 3H-TdR incorporation by con-a-stimulated murine lymphocytes *in vitro*.", Ultrasound Med. Biol., 11, 751-759.

WARD C.A., JOHNSON W.R., VENTER R.D., HO S., FOREST T.W., FRASER W.D. (1983) "Heterogeneous bubble nucleation and conditions for growth in a liquid-gas system of constant mass and volume", J. Appl. Phys., 54, 1833-1843

WILLIAMS A.R. (1983) "Ultrasound: Biological Effects and Potential Hazards." Academic Press, New York.

WILLIAMS A.R., MILLER D.L. (1980) "Photometric detection of ATP release from human erythrocytes exposed to ultrasonically activated gas-filled pores", Ultrasound Med. Biol., 6, 251-256

YAMADA H. (1973) "Strength of Biological Materials", F.G. Evans Ed., Krieger, New York